17th World Conference on Earthquake Engineering, 17WCEE
Sendai, Japan - September 13th to 18th 2020

COMPARISON OF VARIOUS LIQUEFACTION PREDICTIONS BASED ON GROUND INVESTIGATION OF RECLAIMED LAND IN TOKYO BAY

K. Ishikawa (1), S. Yasuda (2)

(1) *Associate Professor, Tokyo Denki University, ishikawa@g.dendai.ac.jp*
(2) *Professor Emeritus, Tokyo Denki University, yasuda@g.dendai.ac.jp*
…

Abstract

During the 2011 Great East Japan Earthquake, the reclaimed land in Tokyo bay was damaged by liquefaction. In this study, a detailed ground investigation is conducted in order to understand the damage mechanism of subsidence and the inclination of detached houses due to liquefaction in Irifune 4-chome, Urayasu city, which suffered major damage after the earthquake disaster. The investigation included conducting questionnaire surveys on liquefaction damage, determining the *N*-value by using a standard penetration test, PS logging, groundwater level measurements, and laboratory tests for undisturbed samples that were collected continuously. This study describes: 1) the relationship between groundwater levels and liquefaction damage using a questionnaire survey; 2) the depth distribution of the liquefaction strength ratio obtained from continuously collected undisturbed samples; and 3) the energy characteristics of each specimen. The characteristics of each method were then evaluated by comparing various liquefaction determinations (i.e., effective stress, the stress-based F_L method, and an energy method). Furthermore, a liquefaction prediction was performed for the Tokyo Bay North Earthquake, which is expected to occur in the future; the duration effect and period characteristics on the liquefaction prediction of the earthquake were evaluated.

In the results of the questionnaire survey, the groundwater level and detached houses damage are correlated. Thus, the inclination and subsidence of detached houses concentrated in the place where the groundwater level was shallower than GL−1.7 m. Moreover, fountain and sand boils due to the liquefaction were witnessed by residents at the points where groundwater levels were shallower than GL−1.4 m. Fountains and sand boils occur early or immediately after an earthquake when the groundwater level is shallow, and the generation is retarded when the groundwater level is deep.

The results of soil investigation showed that the shear wave propagation velocity in the reclaimed land was 80 to 110 m/s and that the soil was loose and essentially silty sand, containing non-plastic fine-grained particles. Furthermore, there was no regularity in the silt content in the reclaimed land at any depth, and the ground was considerably heterogeneous. The depth at which the liquefaction strength was lowest was near the boundary between the reclaimed soil and alluvial sand. The cumulative dissipation energies of each specimen were calculated according to Kokusho [1]. In addition, the liquefaction strength ratios were compared, and a unique relationship, regardless of the difference of ground materials, was found. This, however, does not harmonize with the experimental results of the reconstituted sample.

In the results of liquefaction prediction, the rise process of excess pore water pressure by the effective stress analysis was almost entirely consistent with the eyewitness testimony of the in habitants. A difference in the evaluation result between F_L method and energy method was noted; in the F_L method, the F_L value decreases with depth, whereas in the energy method, it tends to liquefy easily with shallower depths. Thus in the liquefaction prediction, earthquake ground motion of long duration such as that of the Great East Japan Earthquake is a more severe external force for liquefaction than the assumed Tokyo Bay North Earthquake.

Keywords: reclaimed land; undisturbed sample; liquefaction prediction; cumulative dissipation energy

1. Introduction

The 2011 Great East Japan Earthquake caused serious damage associated with liquefaction over a wide area of reclaimed land in the Tokyo Bay area. The characteristics of this earthquake were such that the maximum acceleration in the Tokyo Bay area was not large, but the duration of seismic motion was very long because of the magnitude of 9.0. The authors carried out a field survey and questionnaire after the earthquake, and assessed the actual condition of the damage [2]. It was considered that the liquefaction damage was aggravated by the very long duration of the seismic motion, and the effect of this seismic waveform on the strength of liquefaction was evaluated by laboratory testing. Then, it was proposed that the liquefaction prediction method for long-duration earthquake motions could be rationalized using the correction factors obtained in laboratory tests [3]. In comparison, it was described by Kazama et al. [4] and Kokusyo [1] that liquefaction prediction can be carried out uniformly using energy as an index for various earthquake motions, such as trench-type earthquakes with long durations and crustal earthquakes with short durations but large amplitudes.

In this study, the depth distribution of the liquefaction strength ratio obtained from undisturbed samples collected continuously in Irifune 4-chome, Urayasu City, which was severely damaged by the Great East Japan earthquake, and the energy characteristics of each depth and specimen were evaluated. Then, various liquefaction predictions (effective stress analysis, the stress based method (F_L), and the energy method) were carried out for this site, and the features of each method were evaluated by comparing each prediction result with the actual damage conditions indicated by the questionnaire survey results.

2. Distribution of groundwater level and liquefaction damage in the study area

Groundwater level measurement and questionnairing were carried out in a district where damage to detached houses was concentrated. Figure 1 shows the damage in Urayasu City [5]. Damage to detached houses caused by liquefaction was concentrated in the Nakamachi area, which is reclaimed land. In the Motomachi area, which is a natural sedimentary ground, liquefaction damage has not been confirmed. Figure 2 shows the distribution of groundwater level in Irifune 4-chome measured after the earthquake (May－August 2013). In this area, the groundwater level is shallow near the revetment constructed in the Nakamachi development. The water level tends to gradually increase away from the northeast sea. Comparing the distribution of the groundwater level with the damage distribution of detached houses shown in Fig. 1, it is found that the groundwater level differs by about 1.0 m, especially between in the area with severe damage (along the old revetment) and the areas with little damage (along northwest road).

Figure 3 shows a comparison between the groundwater level in residential areas and the degree of damage to detached houses. The relationship between the groundwater level and damage was as follows: large-scale half collapsed, −1.1 m; half collapsed, −1.2 m; partially damaged, −1.3 m; and undamaged, −1.7 m. In May 2011, the Japanese Cabinet announced a new standard for the evaluation of damage to houses based on two factors, settlement and inclination. A new class of "large-scale half collapsed" was introduced, and houses tilted at angles of more than 1⁄20, 1⁄20 to 1⁄60, and 1⁄60 to 1⁄100 were considered to be completely collapsed, large-scale half collapsed, and half collapsed, respectively. The damage caused to detached houses tended to be greater when groundwater levels were shallow. In our study, no liquefaction-related damage was confirmed when the groundwater level was greater than −1.5 m. However, groundwater level measurements included volume compression settlement by liquefaction. The volume compression settlement by liquefaction was about 20 cm [6], and at the time of the earthquake, the groundwater level was about −1.7 m. The seasonal variation in the groundwater level of this area is shown in Fig. 4. The tendency for the groundwater level to change in relation to rainfall was confirmed. The groundwater level in May and June was −0.7 m to −0.8 m. The groundwater level during the summer season in July and August was −0.9 m to −1.0 m. Groundwater levels were very shallow during the autumn rainy season in September and October, when they were nearly −0.3 m to −0.6 m. After the autumn rainy season, the groundwater level dropped to nearly −0.8 m to −1.1 m. Comparison of the groundwater levels during an autumn rainy season, a summer

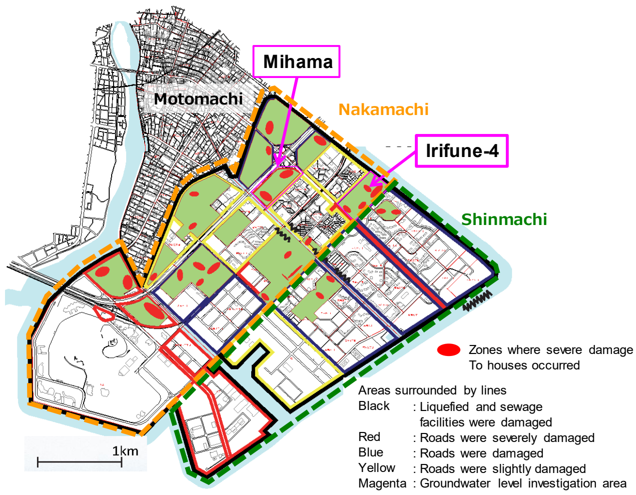

Fig. 1 Liquefaction damage distribution in Urayasu City [5]

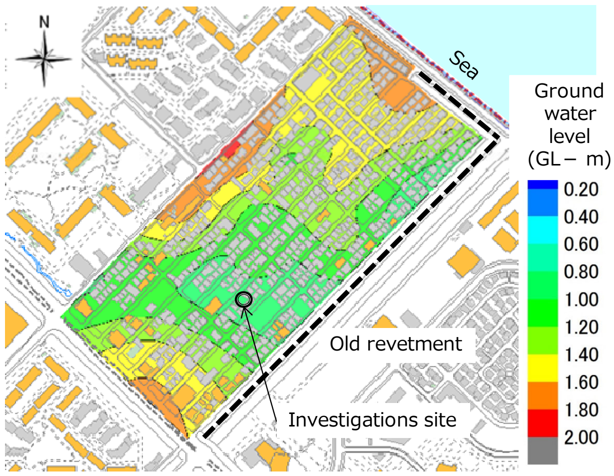

Fig 2 Distribution of groundwater level in Irifune 4-chome

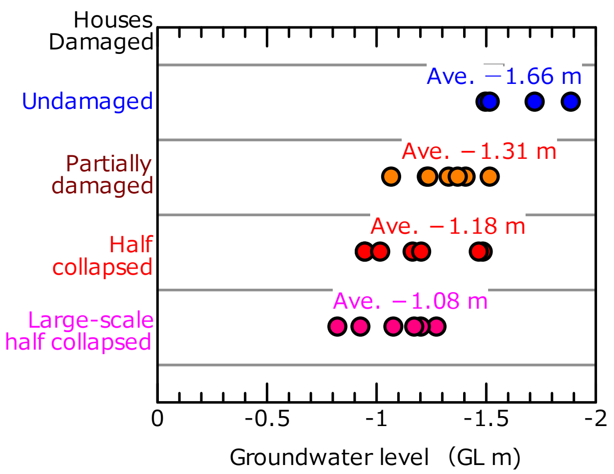

Fig. 3 Relationship between groundwater levels and damage to detached houses

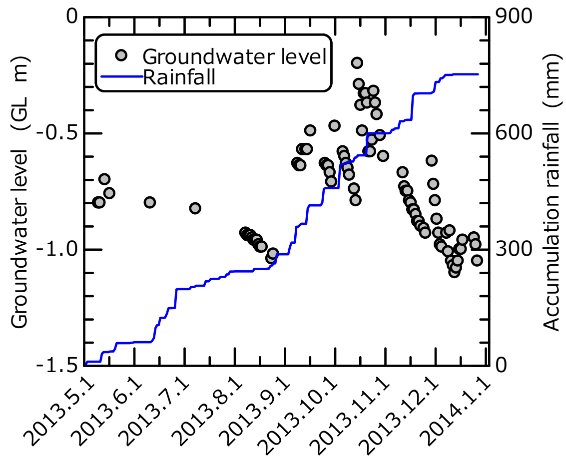

Fig. 4 Seasonal variation of the groundwater level

season, and a winter season confirmed an approximate change of 0.8 m. It is considered that the groundwater level at the time of the earthquake was average.

Figure 5 shows the relationship between the groundwater level and the occurrence time of fountains and sand boils after the main shock and aftershock (for a total of 21 houses). The main shock occurred at 14:46 local time, and the largest aftershock occurred at 15:15 off the coast of Ibaraki Prefecture. Fountains and sand boils were generated in about 60% of the residential land with a groundwater level of about −1.0 m immediately after the main shock. Where the groundwater level was slightly deeper, the generation time tended to be slightly delayed. In addition, where the groundwater level was deeper, the area where fountains and sand boils did not occur increased. The fountains and sand boils after the aftershock occurred immediately after the aftershock in the shallow groundwater level area, whereas there was a delay of only a few minutes after the aftershock in the deep groundwater level of −1.7 m.

Based on the actual conditions of the damage to detached houses caused by liquefaction, the groundwater level at the site, and the behavior of fountains and sand boils at the time of the earthquake

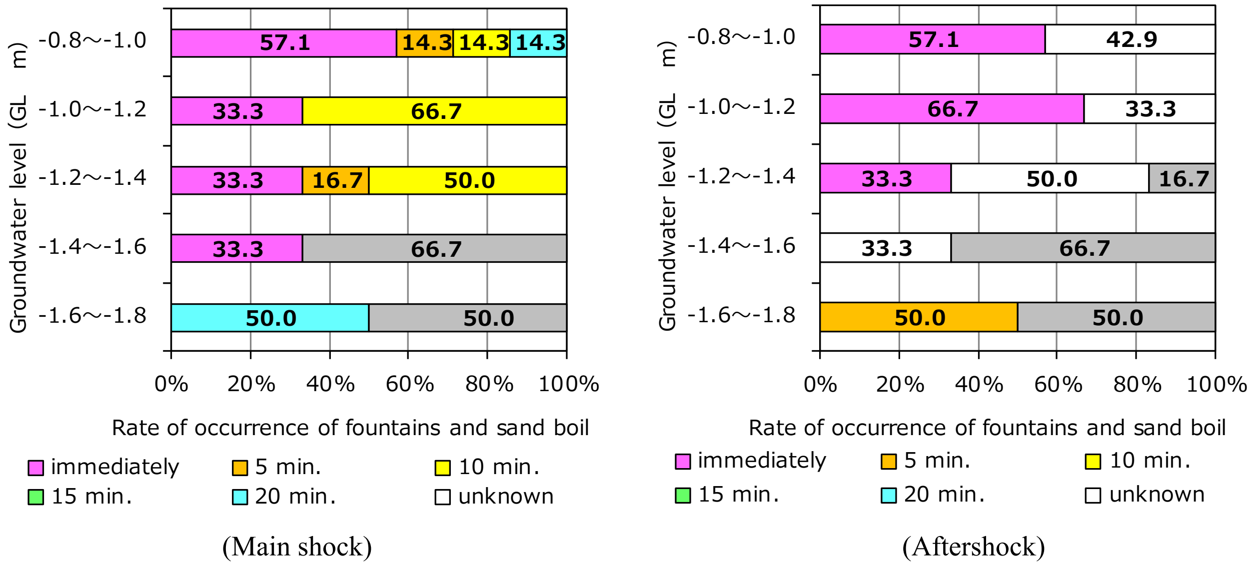

Fig. 5 Relationship between the groundwater level and the occurrence times of fountains and sand boils after the main shock and aftershock (affecting a total of 21 houses).

disaster, the liquefaction layer was identified. The penetrate settlement and inclination of the detached houses depend on the thickness of the layer shallower than the groundwater level and the shear modulus. However, when the stratum below the groundwater level is liquefied, not only does the pore water pressure of the stratum rise, but also the saturation degree of the surface layer is changed by the propagation of the excess pore water pressure to the upper layer. The change caused by excess pore water pressure does not propagate homogeneously, but propagates by stirring of the soil, which is easily propagated in the stratum.

Based on the above results, the average groundwater level at the site where the liquefaction prediction was carried out was inferred to be as shallow as −0.8 m. The surface layer under the houses changed to a state close to saturation because of the excess pore water pressure and the pore water squeezed out from the liquefied layer, and the liquefaction was accelerated by the aftershock. For the liquefaction layer estimated from this damage mechanism, it was judged that the surface layer around −2.0 m under the foundations of the detached houses was liquefied.

3. Ground characteristics based on detailed ground investigation

3.1 Outline of ground investigation

The ground investigation was carried out at the location shown in Fig. 2. The situation occurred immediately after the earthquake when sand boils were generated by liquefaction. The fountains and sand boils continued until the aftershocks 30 minutes later, and water flooding occurred during the aftershocks. The sand boils subsided in the evening of the day of the earthquake. The maximum amount of sand was about 30 cm, and the subsidence of the house was up to 23 cm.

The investigation consisted of boreholes, standard penetration tests, and PS logging, and continuous sampling was carried out from the reclaimed layer to the Holocene sand layer at different hole. Figure 6 shows a borehole column diagram of the study site and the depth distribution of the shear wave velocity. “Tw,” “Tr,” and “GP” in the figure indicate the sampling method and sample number at the indicated depth: Tw indicates hydraulic thin-wall tube sampling, Tr denotes triple-tube sampling, and GP represents gel-push triple-tube sampling [7].

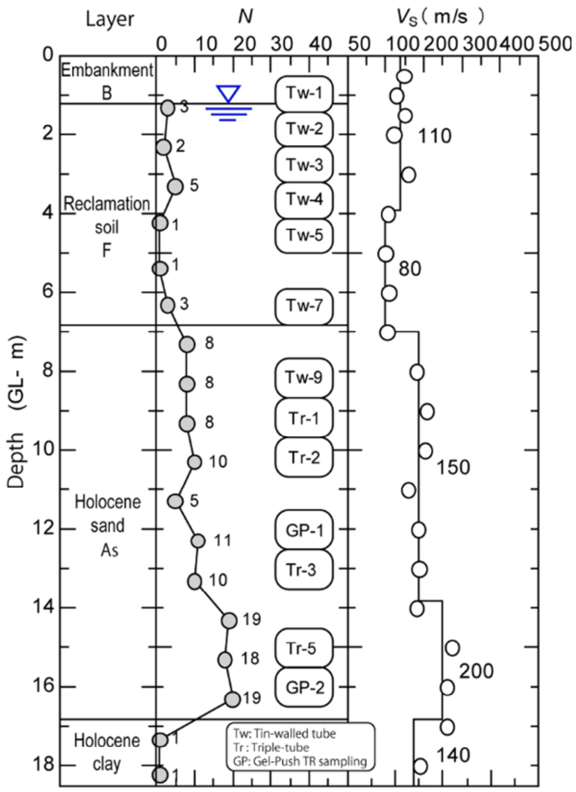

Fig. 6 Borehole column diagram of the study site and depth distribution of shear wave velocity

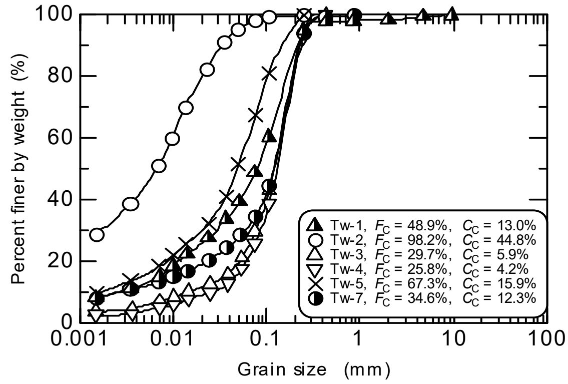

Fig. 7 Grain size distribution curve of the embankment and reclaimed land layer

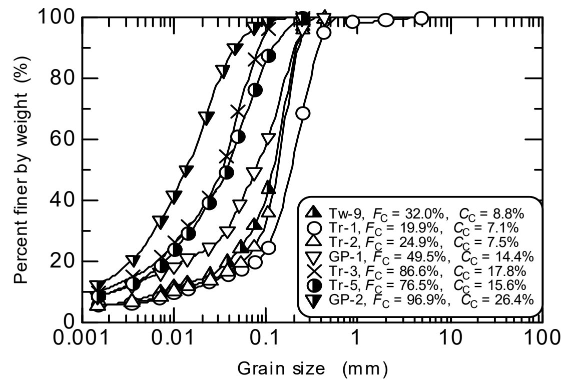

Fig. 8 Grain size distribution curve of the embankment and reclaimed land layer

Layer compositions were determined based on sampling, *N*-values, and shear wave velocity. The embankment layer (layer B) consists of fine sand and silt, and the layer thickness is 1.2 m. The reclaimed land layer (layer F) consists of silt and fine sand, with a layer thickness of 5.6 m. The *N*-value was 1 to 5, and the shear wave velocity was slow at 80 to 110 m/s. The Holocene sand layer (As layer) is homogeneous fine sand and silty sand with a layer thickness of 10 m. The *N*-values were 8 to 19, and the shear wave velocity was 150 to 200 m/s, which was higher than the reclaimed land layer. In addition, the groundwater level at the time of the boring survey was −1.23 m and was located near the boundary between the embankment layer and the reclaimed land layer.

3.2 Physical properties of the sample

Fig. 7 shows the grain size distribution curve of the embankment and reclaimed land layer, representing the physical characteristics of the collected samples, and Fig. 8 shows the grain size distribution curve of the Holocene sand layer. Tw-2 from the reclaimed land layer had a fine fraction content (F_C) of about 98%, a clay content (C_C) of about 45%, and a high plastic index of about 41. Tw-3 to Tw-7 had F_C of 25–67% and C_C of 4–16%, the fine-grained soil contained in the sample was predominantly silt, and the plastic index was characterized by predominantly fine-grained sand with non-plastic granules. Tw-9 to GP-1 from the Holocene sand layer, had F_C of 20–50% and C_C of 8–14% with fine-grained sand, and that the grain size characteristics of Tr-3 to GP-2 near the boundary with the Holocene clay layer changed to sandy clay–clay. In both samples, the plastic index was non-plastic, and the fine granule content was mainly characterized by silt.

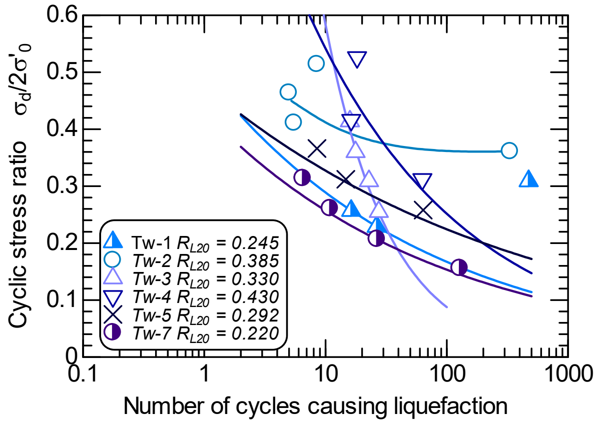

Fig. 9 Liquefaction test results of the reclamation soil

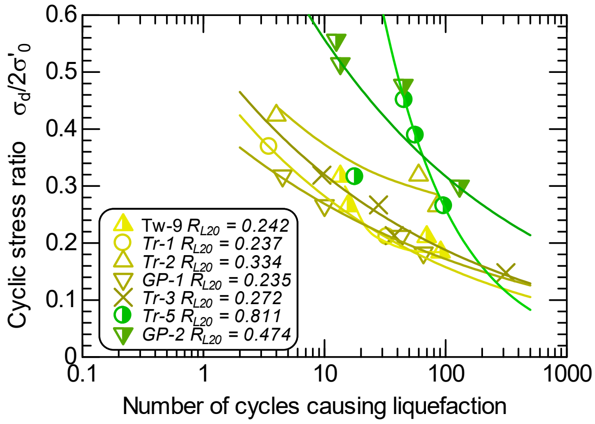

Fig. 10 Liquefaction test results of the Holocene sandy soil

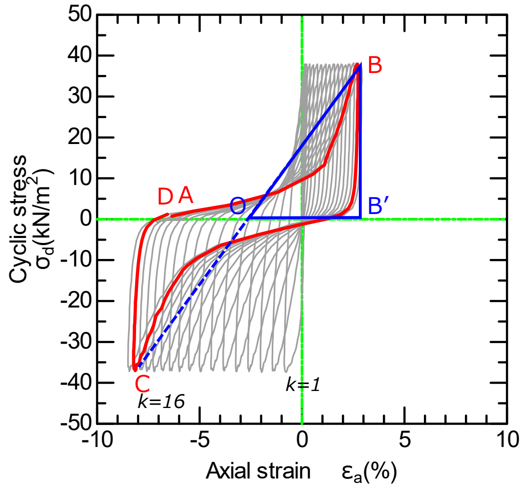

Fig. 11 Stress–strain relationship for sample Tw-7

3.3 Characteristics of the liquefaction strength of each sample

The liquefaction strength of the samples was examined through a cyclic triaxial test. When each specimen was extracted from its sampling tube, visual sample observation was carried out and liquefaction was examined for the same type of specimen in each tube. This was done because the reclamation soil layer may be affected by construction methods and was deposited in a heterogeneous manner. The back pressure 200 kN/m^2 was applied to increase the degree of saturation of the specimen. It was confirmed that the B value (i.e., the ratio of the increment in isotropic stress and excess pore water pressure) was more than 0.95, and consolidation was carried out under an isotropic stress state at the effective overburden pressure for each sample depth. However, Tw-1 was under a stress higher than the effective overburden pressure because of the limitation of the test equipment. Cyclic loading was applied using a sine wave at a frequency of 0.1 Hz after the end of consolidation.

The liquefaction test results of the reclamation soil and sandy layers are shown in Figure 9 and Figure 10, respectively. The data points in the figures represent liquefaction strength, and the horizontal axis represents the number of cycles for a double amplitude axial strain of 5%. Based on the liquefaction strength curves, the stress ratio for which the number of cycles is 20 is defined as the liquefaction strength ratio. These results show that the liquefaction strength ratio in the reclamation soil layer varied between 0.220 and 0.430 with depth and exhibited characteristics that were different for each liquefaction strength curve. The

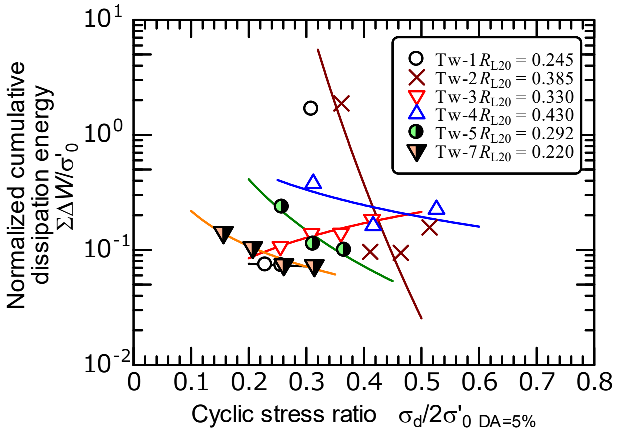

Fig. 12 Relationships between the cyclic stress ratio and cumulative dissipation energy

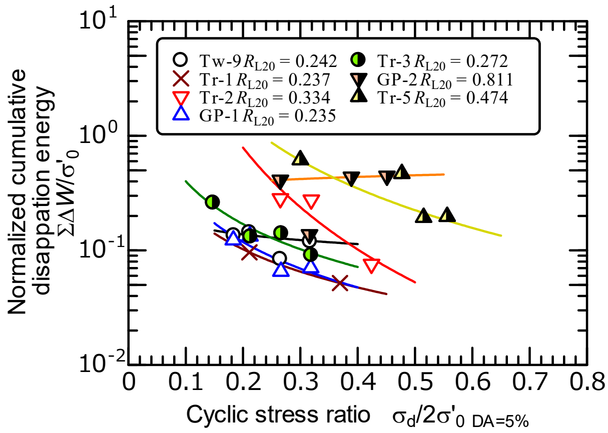

Fig. 13 Relationships between the cyclic stress ratio and cumulative dissipation energy

liquefaction strength ratio in the Holocene sandy soil layer varied slightly from 0.235 to 0.334 with depth. Moreover, the characteristics of the liquefaction strength curves exhibited almost the same tendency. However, the specimen at the bottom of this layer had larger *N*-values than those at other depths, the shear-wave velocity was 200 m/s, and the liquefaction strength ratios were 0.474 to 0.811, including considerably large values for several fine-grained soils.

3.4 Energy evaluation of the liquefaction characteristics of each sample

Based on the results of the liquefaction test for each sample shown in the previous section, the cumulative dissipation energy ($\Sigma\Delta W$) and the cumulative strain energy (ΣW) were calculated to investigate the liquefaction characteristics in terms of energy. Although Fig. 11 shows an example of the stress–strain relationship for sample Tw-7 the dissipation energy ΔW was calculated by cumulating the historical area of the stress–strain relationship (*ABCD*) for each cycle to an arbitrary cycle for each number of cycles. The strain energy W was determined by calculating the middle point (*O*) of the line portion connecting the vertex (*BC*) of the hysteresis loop of the stress–strain relationship and accumulating the area of the triangle *OBB*'.

Fig. 12 shows the relationship between the cyclic stress ratio at 5% of the double amplitude axial strain of each specimen of the embankment and reclamation soil layer and the cumulative dissipation energy at that time, divided by the effective confining pressure, resulting in the normalized cumulative dissipation energy ($\Sigma\Delta W/\sigma'_0$). Fig. 13 shows the results for the specimens of the Holocene sand layer in the same manner as the embankment and reclamation soil layers in the previous figures. Therefore, for each specimen, a smaller cyclic stress ratio tended to be associated with a larger value of $\Sigma\Delta W/\sigma'_0$. This finding indicates that a specimen with a low cyclic stress ratio would have large cumulative energy dissipation before strain developed significantly. In addition, the characteristics of the difference in the liquefaction strength ratio R_{L20} is that a smaller R_{L20} value is associated with a smaller $\Sigma\Delta W/\sigma'_0$, whereas a larger R_{L20} is associated with a larger $\Sigma\Delta W/\sigma'_0$.

Fig. 14 shows the relationship between R_{L20} and $\Sigma\Delta W/\sigma'_0$. The $\Sigma\Delta W/\sigma'_0$ at R_{L20} shows the approximate curve of the samples shown in Fig. 12 and Fig. 13. From this, it can be seen that the relationship between the embankment and reclamation soil layer and the Holocene sand layer is almost unique, and the black line in Fig. 14 shows the approximate curve obtained from the results of tests by Kokusho [1]. However, the relationship between them in this experiment tended to be stronger than that indicated by previous experiments.

Fig. 15 shows the relationship between the normalized cumulative dissipation energy ($\Sigma\Delta W/\sigma'_0$) and the normalized cumulative strain energy ($\Sigma W/\sigma'_0$), in which the relationship between $\Sigma\Delta W/\sigma'_0$ and $\Sigma W/\sigma'_0$ at

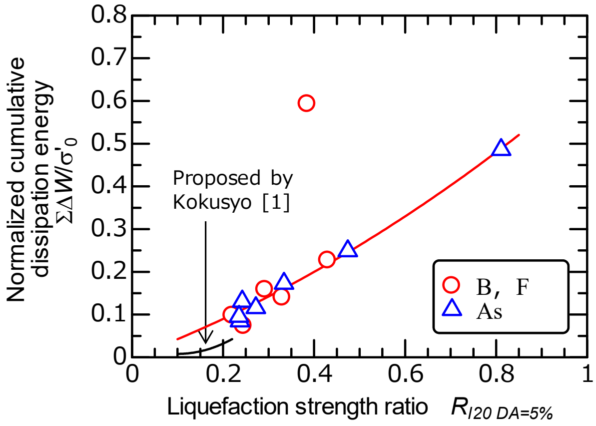

Fig. 14 Relationship between R_{L20} and $\Sigma\Delta W/\sigma'_0$

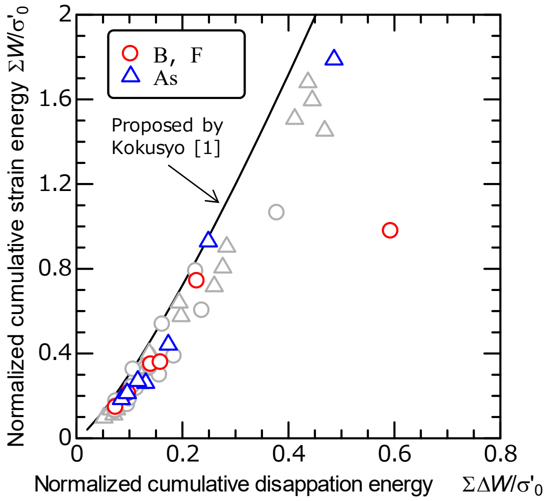

Fig. 15 Relationship between the normalized cumulative dissipation energy and the normalized cumulative strain energy

the time when the axial strain amplitude of each specimen was 5% is plotted in gray, and colors represent the relationship corresponding to R_{L20}, indicating that the relationship between the two is almost linear; the black line in the figure shows the proposed line from the results of Kokusho. However, the relationship between the two is distributed to the right of the historical test results. This discrepancy can be attributed to differences in the conditions of the specimen and the cyclic stress ratio. Whereas previous studies used reconstituted samples containing non-plastic fine grains for clean sands, sampling samples were used in this study. The range of cyclic stress ratios used in the liquefaction test was 0.148–0.811 in this study, compared with 0.082–0.313 in the experiments on reconstituted samples, with different stress-specific amplitudes. However, regardless of the differences in density and fine fraction contents of each specimen, as in previous experiments, there was no change in the unique relationship between the cumulative dissipation energy and the strain energy that needed to be provided externally, corresponding to internal energy loss.

4. Liquefaction prediction using detailed ground investigation results

4.1 Outline of liquefaction prediction

The seismic waveforms used for liquefaction prediction are shown in Fig. 16. The seismic waveform assumed for the Great East Japan Earthquake was calculated by combining the observed waveform of the main shock at the K-net Urayasu station [8] with the aftershock observed 30 minutes later and deconvoluting it back to the engineering base to determine the input seismic waveform. The Tokyo Bay North Earthquake is a strong seismic waveform in the engineering base of the region prepared by the Special Committee on Tokyo Inland Earthquake Countermeasures of the Central Disaster Management Council [9]. Characteristically, the maximum acceleration of the waveform of the Great East Japan Earthquake is not very large, but the frequency of repetition is high because of the long duration. However, the Tokyo Bay North Earthquake waveforms have a high maximum acceleration and a short duration.

YUSAYUSA-2 was used for effective stress analysis [10], and the liquefaction characteristics of each layer were set based on the results in Figs. 9 and 10. The water permeability coefficient was set as the maximum value of each layer obtained by the estimation equation of Morita et al. [11] based on the particle size characteristics of the samples. The values were the maximum values of the embankment layer (5.0E-7 m/s), the reclamation layer (1.0E-4 m/s), and the Holocene sand layer (the upper part: 1.0E-5 m/s, the lower part: 1.0E-6 m/s). This was because the reclaimed ground has non-uniform grain size characteristics, and the

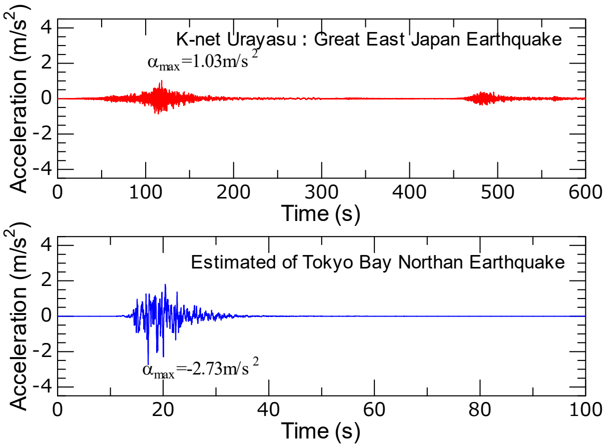

Fig. 16 Seismic waveforms used for liquefaction prediction [8], [9]

Tabel 1 F_{L} method under the four conditions

Case	Method	Force	Earthquake shear strength ratio
A-1	**Highway bridge specifications** $\boldsymbol{F_L = C_W R_{L20}/L}$ Seismic characteristics; $C_W = 0.59 \times R_{L20}{}^{-0.25}$: Great East Japan Eq. $C_W = 1.0$: Tokyo Bay North Eq. Earthquake shear strength ratio; *Simplified* $L = (1.0 - 0.015Z)(\alpha_{max}/g)(\sigma_V/\sigma'_V)$ *Detailed* $L = \tau_{max}/\sigma'_V$	**Great East Japan Eq.**	Simplified method **Estimated at Max. acceleration**
A-2			Detailed method **Estimated at Max. shear stress at each depth**
A-3		**Tokyo Bay North Eq.**	Simplified method **Estimated at Max. acceleration**
A-4			Detailed method **Estimated at Max. shear stress at each depth**
B-1	**Guidelines for building foundation design** $\boldsymbol{F_L = R_{L15}/L}$ Seismic characteristics; $M = 9.0$: Great East Japan Eq. $M = 7.5$: Tokyo Bay North Eq. Earthquake shear strength ratio; *Simplified* $L = 0.1(M-1)(\alpha_{max}/g)(\sigma_V/\sigma'_V)(1-0.015Z)$ *Detailed* $L = 0.1(M-1)\tau_{max}/\sigma'_V$	**Great East Japan Eq.**	Simplified method **Estimated at Max. acceleration**
B-2			Detailed method **Estimated at Max. shear stress at each depth**
B-3		**Tokyo Bay North Eq.**	Simplified method **Estimated at Max. acceleration**
B-4			Detailed method **Estimated at Max. shear stress at each depth**

propagation of excess pore water pressure was assumed to be the water supply where the permeability coefficient was the highest. The groundwater level was set to −0.8 m as the average groundwater level.

The simple liquefaction prediction method was determined by the F_{L} method under the four conditions shown in Table 1. Case A is a prediction method for the highway bridge specifications [12], and Case B is a prediction method on the recommendations for design of building foundations [13]. Both are common liquefaction prediction methods used in Japan.

Liquefaction prediction by the energy method was performed in accordance with the method proposed by Kokusho [1]. In this method, the upward energy received by the ground was required because of the input earthquake ground motion, and the cumulative value of the seismic wave upward energy was used to evaluate the time history of the ascending wave velocity at each layer obtained from the seismic response analysis.

4.2 Liquefaction prediction results caused by differences in seismic motion

Figure 17 shows the results of liquefaction prediction by effective stress analysis. The Great East Japan Earthquake succeeded in reaching the effective overburden pressure at the top of the reclamation soil layer (F-1 and F-2 layers) because of the dissipative propagation of excess pore water pressure generated at the time of the main shock and the aftershock. However, it was found that the Tokyo Bay North Earthquake did not cause excessive pore water pressure leading to liquefaction across the entire layer. Figure 18 shows the liquefaction predictions results from the F_{L} method. The depth distribution of the F_{L} values varies greatly between the simplified method (Cases A-1, A-3, B-1, and B-3) using the maximum surface acceleration as the external force and the detailed method (Cases A-2, A-4, B-2, and B-4) using the shear stress at each depth as external force through seismic response analysis. This factor is influenced by the coefficient of reduction in the depth direction, and it is suggested that with greater depth, liquefaction tends to become more likely when the liquefaction is determined by the simplified method, based on the maximum ground acceleration against the soil conditions where soft ground is thickened and accumulated, such as in Urayasu City. The characteristics of the results of the energy method shown in Fig. 19 differ greatly from those of the F_{L} method in that they are greatly affected by the difference in seismic motion. The Great East Japan Earthquake (long duration, small acceleration) and the Tokyo Bay North Earthquake (short duration, large acceleration) both were associated with easier liquefaction; however, because of the different seismic motion characteristics, although liquefaction was judged to occur in some layers in the assumed Tokyo Bay North Earthquake, the extent of liquefaction was less than that associated with the Great East Japan Earthquake. Another advantage of the energy method is that it is possible to predict liquefaction in consideration of the effects of the main shock and aftershock.

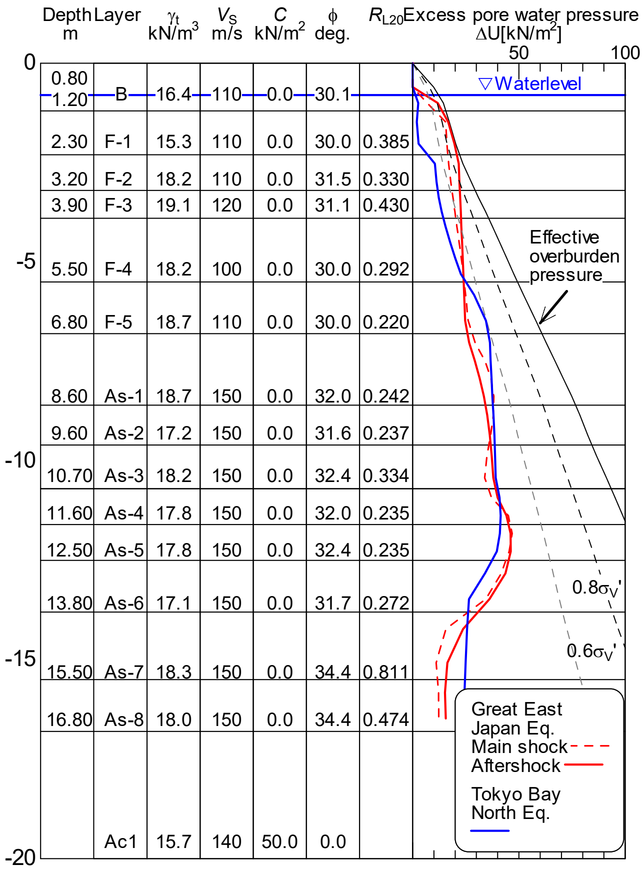

Fig. 17 Results of liquefaction prediction by effective stress analysis

The residents witnessed that the damage at the time of the study was caused by fountains and sand boils immediately after the earthquake, and that the situation continued until the aftershocks. In addition, it was reported that the sand boils continued until the evening of the day of the earthquake. The liquefaction layer, estimated from the actual damage and the damage mechanism of the detached houses, was considered to have affected the surface layer around −3.0 m below the foundation of detached houses. In the Urayasu area, liquefaction damage was confirmed in the reclaimed areas of Nakamachi and Shinmachi, although no damage due to liquefaction was confirmed in the former area. From this, it was inferred that the alluvial sediment layer did not become liquefied. The actual situation of the damage caused by liquefaction and the results of various liquefaction assessments were compared. First, the results of the liquefaction evaluation by the F_L method and those of the energy method differ. The energy method judges that the upper part of the reclamation layer and the alluvial sediment layer (As-1 and As-2 layer) become liquefied, and in particular, it can be judged that the reclamation soil layer is likely to become liquefied, which is the result of the judgment based on the actual situation of the damage. Nonetheless, the ground layer, which was judged to be liquefied by the F_L method using the maximum surface acceleration as the external force, showed the same results in the energy method. However, the depth distribution of F_L becomes smaller as the lower layer, and the alluvial sandy soil layer becomes F_L at the same level as the reclamation soil layer. In addition, the F_L method using the maximum shear stress of each layer based on the seismic response analysis resulted in the judgment of liquefaction in parts of the F-2 and F-5 layers of the reclamation soil layer, but the results of the F_L method differ greatly depending on the difference in the setting of the external seismic force. Comparing the actual situation of the damage with the results of the F_L method using the maximum acceleration, it was interpreted as the result of the judgment on the safety side. However, it was found that the process of the increase in excess pore water pressure caused by YUSAYUSA was largely consistent with the witness

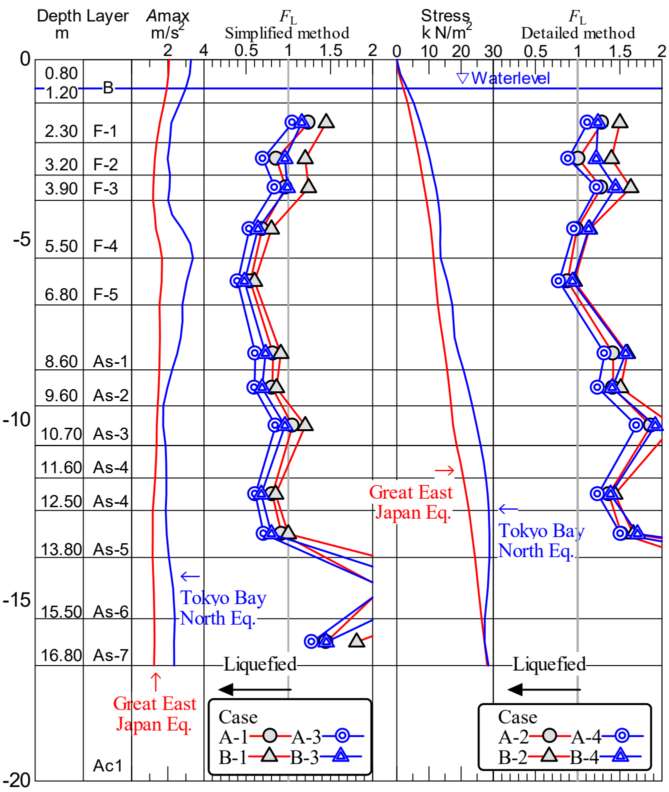

Fig. 18 Results from the F_L method

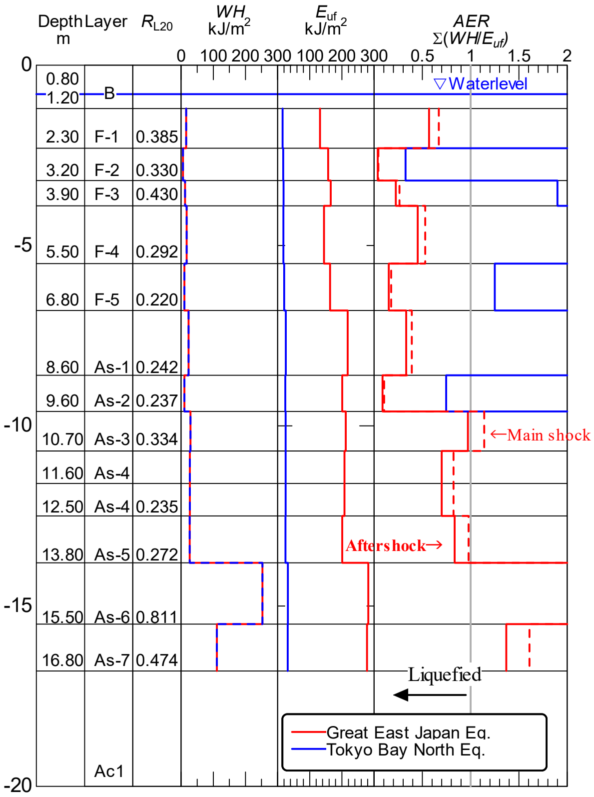

Fig. 19 Results from the energy method

information from the inhabitants, and determination results similar to these characteristics were obtained from the F_L method using the maximum shear stress of each layer as well as the energy method.

Finally, in the liquefaction prediction for the Tokyo Bay North Earthquake assumed to occur in the future, liquefaction was difficult based on the effective stress analysis and energy method, and the F_L simplified method yielded completely different results. This is an issue of the simplified F_L method, and it is necessary to take into account the impact of the reduction coefficient in the depth direction and earthquake ground motion characteristics when making more rational liquefaction-related decisions in the future.

5. Conclusions

In this study, a detailed ground survey was conducted at Irifune 4-chome, Urayasu City, where liquefaction damage occurred during the 2011 Great East Japan Earthquake. The depth distribution of the liquefaction strength characteristics of continuously sampled samples and various liquefaction determinations (effective stress analysis, the stress method (F_L method), and the energy method) were evaluated at the site. The characteristics of each method were compared with the actual conditions of damage determined through questionnaire surveys, and the following findings were obtained.

1) The reclamation soil layer is inhomogeneous, and the liquefaction intensity in the depth direction is highly variable. In addition, it was found that the low liquefaction strength ratios within the reclamation soil layer were near the boundary between the reclamation soil layer and the alluvial sediment layer.

2) When the normalized cumulative dissipation energy was calculated for each specimen, a smaller cyclic stress ratio was associated with a greater value of $\Sigma\Delta W/\sigma'_0$. In addition, the relation between R_{L20} and $\Sigma\Delta W/\sigma'_0$ was almost unique regardless of the difference between the embankment and reclamation soil

layer and the alluvial sediment layer, but the relationship tended to be stronger than that indicated by the experimental results of previously reconstituted samples.

3) In determining liquefaction by the stress method, it is important to appropriately evaluate the coefficient of reduction of the shear stress ratio during earthquakes when determining liquefaction relative to the maximum ground acceleration. The ground characteristics of this study differ from the results based on using the maximum shear stress because the proposed formula used in the road bridge instructions and the building foundation structure design guidelines was used to determine the liquefaction of the alluvial sediment layer. Therefore, it is necessary to appropriately analyze the seismic response in the ground where soft ground, as in this study, is thickened and deposited.
4) In the liquefaction evaluation using the energy method, the upper part of the reclamation soil layer and the alluvial sediment layer (As-1 and As-2 layers) was judged to be liquefied, and it was judged that the reclamation layer was likely to become liquefied.
5) The process of the increase in excess pore water pressure caused by YUSAYUSA was found to be largely consistent with the witness information from the inhabitants and the actual situation of the damage. The determination results similar to these characteristics were based on the F_L method using the maximum shear stress of each layer and the energy method. However, the results of the energy method and the degree of damage are not yet sufficiently verified, and further investigation is therefore necessary.

6. References

[1] Kokusho T (2013): Liquefaction potential evaluations: energy-based method versus stress-based method. *Canadian Geotechnical Journal*, **50** (10), 1088-1099.

[2] Yasuda S, Harada K, Ishikawa K, Kanemaru Y (2012): Characteristics of liquefaction in Tokyo Bay area by the 2011 Great East Japan Earthquake. *Soils and Foundations,* **52** (5), 793-810.

[3] Ishikawa K, Yasuda S, Aoyagi T (2014): Studies on the reasonable liquefaction-prediction method of the 2011 Great East Japan Earthquake. *Japanese Geotechnical Journal*, 9(2), 169-183, in Japanese.

[4] Kazama M, Suzuki T, Yanagisawa E (1999): Evaluation of dissipation energy accumulated in surface ground and its application to liquefaction prediction. *Journal of Japan Society of Civil Engineers*, 631(III-48) 161-177, in Japanese.

[5] Technical Committee on Measures against Liquefaction in Urayasu City (2011): Report on measures against liquef action in Urayasu City, http://www.city.urayasu.lg.jp/shisei/johokoukai/shingikai/shichoukoushotsu/1002796/1002934.html

[6] Yasuda S, Ishikawa K (2015): Effect of lowering the ground water table as the countermeasure against liquefaction-induced damage to houses, *Journal of Japan Association for Earthquake Engineering*, 15 (7), 205-219, in Japanese.

[7] Mori K, Sakai K (2016): The GP sampler: A new innovation in core sampling. *5th International conference on geotechnical and geophysical site characterization*, Keynote. Queensland, Australia.

[8] National Research Institute for Earth Science and Disaster Prevention (NIED) (2011): K-NET WWW service. Japan, http://www.kyoshin.bosai.go.jp/kyoshin/

[9] Cabinet office, Government of Japan (2019): https://www.geospatial.jp/ckan/organization/naikakufu-02

[10] Yoshida N, Towhata I (2003): YUSAYUSA-2, SIMMDL-2, Theory and practice, Revised version (ver. 2.10)

[11] Morita Y, Tsubota K, Nishigaki M, Komatsu M (2004): Proposed new equation for estimating the permeability of soil considering particle size distribution and compaction. *Proceeding of the 39th Japan National Conference on Geotechnical Engineering*, 581, 1159-1160, in Japanese.

[12] Japan Road Association (2017): Specification for Highway Bridges. *Maruzen,* in Japanese.

[13] Architectural Institute of Japan (2010): Recommendations for Design of Building Foundations. *Maruzen,* in Japanese.

